

Compositional phase stability of correlated electron materials within DFT+DMFTEric B. Isaacs^{✉*} and Chris A. Marianetti[†]*Department of Applied Physics and Applied Mathematics, Columbia University, New York, New York 10027, USA* (Received 26 March 2019; accepted 15 July 2020; published 27 July 2020)

Predicting the compositional phase stability of strongly correlated electron materials is an outstanding challenge in condensed matter physics, requiring precise computations of total energies. In this work, we employ the density functional theory plus dynamical mean-field theory (DFT+DMFT) formalism to address local correlations due to transition metal d electrons on compositional phase stability in the prototype rechargeable battery cathode material Li_xCoO_2 , and detailed comparisons are made with the simpler DFT+ U approach (i.e., the Hartree-Fock solution of the DMFT impurity problem). Local interactions are found to strongly impact the energetics of the band insulator LiCoO_2 , most significantly via the E_g orbitals, which are partially occupied via hybridization with O p states. We find CoO_2 and $\text{Li}_{1/2}\text{CoO}_2$ to be moderately correlated Fermi liquids with quasiparticle weights of 0.6–0.8 for the T_{2g} states, which are most impacted by the interactions. As compared to DFT+ U , DFT+DMFT considerably dampens the increase in total energy as U is increased, which indicates that dynamical correlations are important to describe this class of materials despite the relatively modest quasiparticle weights. Unlike DFT+ U , which can incorrectly drive Li_xCoO_2 toward spurious phase separating or charge-ordered states, DFT+DMFT correctly captures the system's phase stability and does not exhibit a strong charge-ordering tendency. Most importantly, the error within DFT+ U varies strongly as the composition changes, challenging the common practice of artificially tuning U within DFT+ U to compensate the errors of Hartree-Fock. DFT+DMFT predicts the average intercalation voltage decreases relative to DFT, *opposite* to the result of DFT+ U , which would yield favorable agreement with experiment in conjunction with the overprediction of the voltage by the strongly constrained and appropriately normed DFT functional.

DOI: [10.1103/PhysRevB.102.045146](https://doi.org/10.1103/PhysRevB.102.045146)**I. INTRODUCTION**

Strongly correlated materials, for which density functional theory (DFT) calculations often break down due to strong electron-electron interactions, are a challenging class of condensed matter systems relevant to several important technologies [1,2]. One example is Li ion rechargeable batteries. These electrochemical cells rely critically on a cathode material that can reversibly intercalate Li ions [3]. Since cathode materials typically are based on transition metal oxides to accommodate changes in oxidation state, they have an open d -electron shell and are susceptible to strong correlation physics.

Currently, the dominant cathode materials are based on Li_xCoO_2 (LCO), a layered compound in which Li ions are intercalated between layers of edge-sharing Co–O octahedra, as shown in Fig. 1(d) [4]. Several early theoretical studies that revealed significant insight into the electronic structure and phase diagram of LCO [5–8] were based on DFT [9,10], the *de facto* standard for first-principles calculations in solid-state physics and chemistry. It is not uncommon, however, for DFT to fail to capture the physics of correlated materials due to the approximation for the exchange-correlation functional [e.g., local density approximation (LDA) or generalized gradient approximation (GGA)].

While DFT calculations in many ways reliably characterize LCO, there are deficiencies in their description. DFT (GGA) underestimates the intercalation voltage by around 0.8 V [11]. In addition, using a plane-wave basis set and ultrasoft pseudopotentials, Van der Ven *et al.* found that LDA overestimates the order-disorder transition temperature for $x = \frac{1}{2}$ by 100 °C [8]. We note that the LDA linear augmented plane-wave results of Wolverton and Zunger [7] do not show the same overestimation, though this study uses only roughly one third as many DFT calculations to parametrize the cluster expansion, in addition to performing slightly restricted structural relaxations.

One widely utilized approach to go beyond DFT is the DFT+ U method [12], in which an explicit onsite Coulomb interaction U is added to account for the strong interactions in the d shell along with a simple mean-field ansatz for the energy functional. However, DFT+ U does not fully remedy the shortcomings of DFT and in some cases hurts the description more than it helps. DFT+ U still underestimates the voltage by 0.3 V, and it can overestimate the order-disorder transition temperature by as much as several hundred degrees [13]. DFT+ U drives LiCoO_2 toward a high-spin transition [14] not observed in experiments [15–17] and, unless spurious charge ordering is permitted to occur, incorrectly predicts phase separation [13,18]. Moreover, DFT+ U finds CoO_2 to be an insulator in disagreement with experiment [19]. DFT+ U clearly is problematic in the context of LCO.

Here, we revisit the electronic structure, voltage, and phase stability of LCO using more sophisticated DFT plus

*Present address: Department of Materials Science and Engineering, Northwestern University, Evanston, IL 60208, USA.

[†]chris.marianetti@columbia.edu

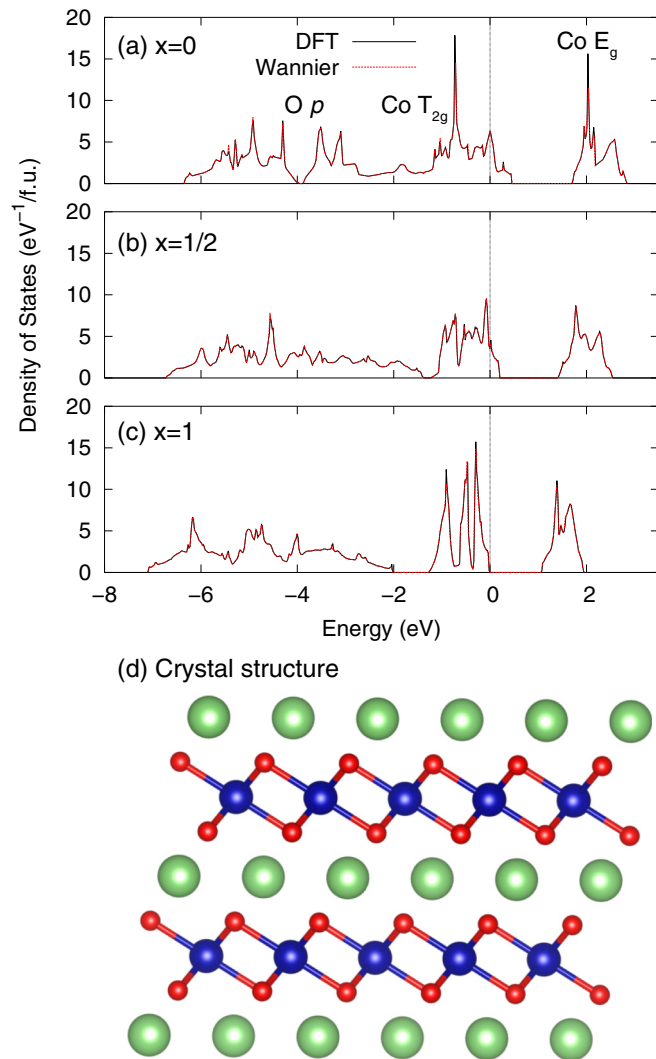


FIG. 1. Density of states for DFT (black solid lines) and using the Wannier basis (dotted red lines) for (a) metallic CoO_2 , (b) metallic $\text{Li}_{1/2}\text{CoO}_2$, and (c) band insulator LiCoO_2 . The Fermi level (valence band maximum for $x = 1$) is indicated by the vertical dotted black line. (d) Crystal structure of LCO with O3 layer stacking with all the Li shown ($x = 1$). The large green, medium blue, and small red spheres represent ionic positions of Li, Co, and O, respectively. The image of the crystal structure is generated using VESTA [61].

dynamical mean-field theory (DFT+DMFT) calculations [20] based on GGA. In this framework, the many-body DMFT approach captures the dynamical local correlations of Co d electrons embedded in the crystal, whereas only the static effects are described within DFT+ U . Total energy DFT+DMFT calculations have become an important tool for understanding structural stability of materials with electronic correlations [21–43], and our work extends this exploration to the realm of compositional phase stability.

We find that DFT+DMFT describes LiCoO_2 as a band insulator with modest shifts and broadenings of the low-energy spectrum, most prominently via the E_g levels partially occupied via hybridization with O p states. CoO_2 and $\text{Li}_{1/2}\text{CoO}_2$ are Fermi liquids whose T_{2g} states are most strongly affected by the interactions, with quasiparticle weight

of around 0.6–0.7. DFT+DMFT, unlike DFT+ U , does not strongly stabilize charge ordering in $\text{Li}_{1/2}\text{CoO}_2$, nor does it predict insulating behavior for CoO_2 or $\text{Li}_{1/2}\text{CoO}_2$; in other words, DFT+DMFT substantially improves the description of the electronic structure. Dynamical correlations significantly dampen the impact of U on the total energy of LCO, but more substantially for CoO_2 than LiCoO_2 , leading to a reduction in voltage as compared to DFT, whereas DFT+ U yields the qualitatively opposite behavior. Given the more accurate strongly constrained and appropriately normed (SCAN) DFT functional overestimates the experimental voltage, such a decrease in the predicted voltage is expected to lead to agreement between experimental and predicted voltage for DFT+DMFT based on the SCAN functional. Similar to the voltage behavior, the $x = \frac{1}{2}$ formation energy prediction is significantly affected by dynamical correlations: unlike DFT+ U , DFT+DMFT only weakly influences the formation energy of $x = \frac{1}{2}$ as compared to DFT. Our results demonstrate the importance of dynamical correlations, missing in DFT+ U , to accurately describe the electronic structure and energetics of correlated electron materials.

II. COMPUTATIONAL DETAILS

We perform single-site paramagnetic DFT+DMFT total energy calculations using the formalism of Ref. [36] based on the spin-independent GGA of Perdew, Burke, and Ernzerhof (PBE) [44] and the projector augmented-wave (PAW) method [45,46] as implemented in the VASP code [47–50]. Select calculations are also performed using the SCAN functional [51]. Given that LCO exhibits no long-range magnetic order in experiment [52], the paramagnetic state is justified and we do not search for long-range magnetic order. The structures are fixed to the fully relaxed spin-dependent DFT ground state structures with O3 layer stacking [8], corresponding to a band insulator for $x = 1$ and ferromagnetic low-spin metals for $x = 0$ and $\frac{1}{2}$. Except where otherwise noted, calculations are performed using the fixed non-spin-polarized DFT charge density, i.e., they are non-charge-self-consistent (NCSC); this is done for reasons of computational efficiency. We characterize the magnitude of the error associated with charge self-consistency by directly comparing NCSC and charge-self-consistent (CSC) calculations within DFT+ U , demonstrating that the error is sufficiently small for the trends we are studying in this paper. A 500-eV energy cutoff and k -point meshes of k -point density corresponding to $9 \times 9 \times 9$ for the rhombohedral LiCoO_2 primitive cell and $19 \times 19 \times 19$ for the bulk Li primitive cell are employed. The ionic forces and total energy are converged to $0.01 \text{ eV}/\text{\AA}$ and 10^{-6} eV , respectively.

To define the correlated subspace, we utilize the maximally localized Wannier function (MLWF) basis [53] for the full p - d manifold and perform a unitary rotation of the d orbitals to minimize the off-diagonal hoppings [36]. The Slater-Kanamori (SK) interaction with J_{SK} set to 0.7 eV is employed, and we use the numerically exact hybridization expansion continuous-time quantum Monte Carlo (CTQMC) solver for the five-orbital impurity problem [54,55] at temperature $T = 290 \text{ K}$. For DMFT, we perform calculations using density-density interactions. In order to assess the impact of terms beyond density-density interactions, we also perform

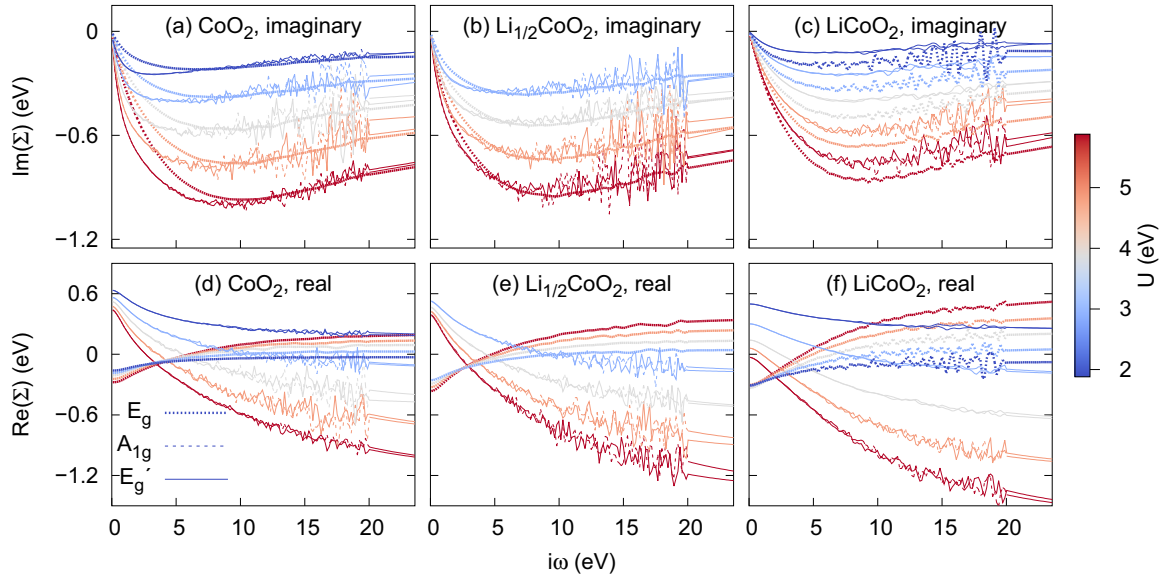


FIG. 2. Imaginary part of the DMFT self-energy on the imaginary frequency axis for (a) CoO_2 , (b) $\text{Li}_{1/2}\text{CoO}_2$, and (c) LiCoO_2 with density-density interactions for different values of U . Solid, dashed, and dotted lines correspond to the E'_g , A_{1g} , and E_g orbitals. (d)–(f) Show the corresponding real parts referenced to the chemical potential.

calculations augmenting density-density interactions with the off-diagonal J terms within the E_g manifold, in which the impact of off-diagonal J is expected to be most important due to the partial filling of E_g . For comparison, we also perform DFT+ U calculations using the projector (corresponding to projection onto spherical harmonics within the PAW spheres [56]) correlated subspace in VASP (LDAUTYPE=4) and present all our results in terms of the U and J corresponding to this interaction model via $U = U_{\text{SK}} - 8J_{\text{SK}}/5$ and $J = 7J_{\text{SK}}/5$ [57]. Although it has limitations such as lack of normalization [58,59], we consider the projector correlated subspace since it is widely used. It should be noted that J is fixed in all calculations, even though a range of different U is explored. We employ the fully localized-limit (FLL) form of the double counting [60]. The total energy is converged to within ~ 10 meV/f.u. for the DMFT self-consistency condition.

III. RESULTS AND DISCUSSION

A. Electronic structure of CoO_2 and LiCoO_2

We begin by studying the basic electronic structure of LiCoO_2 and CoO_2 as a function of U , allowing for a direct comparison between DFT+DMFT and DFT+ U . Corresponding results for $\text{Li}_{1/2}\text{CoO}_2$ are included, but these are not directly discussed until Sec. III C. In LCO, the ability of the oxygens to relax in the out-of-plane direction slightly distorts the CoO_6 octahedra and results in a symmetry lineage of $T_{2g} \rightarrow A_{1g} + E'_g$ relative to cubic symmetry, though we will still sometimes refer to this manifold as T_{2g} for brevity. The DFT density of states is shown in Figs. 1(a) and 1(c) for CoO_2 and LiCoO_2 , respectively. Within DFT, LiCoO_2 is a band insulator with nominally filled T_{2g} and empty E_g states, whereas CoO_2 is metallic with a hole in the T_{2g} manifold. The density of states from the Wannier correlated subspace for the full p - d manifold, shown in the dashed red lines, is numerically

identical to that of DFT by construction. The Wannier functions are well localized with values for the spread $\langle (\mathbf{r} - \bar{\mathbf{r}})^2 \rangle$ of around 0.42 and 0.45 \AA^2 for the individual Co d orbitals of CoO_2 and LiCoO_2 , respectively.

An essential quantity in Green function based approaches is the self-energy, which is central to computing the total energy and determining the low-energy properties. The electronic self-energy Σ on the imaginary (Matsubara) frequency axis obtained via the CTQMC solver is shown for CoO_2 and LiCoO_2 in Fig. 2 for density-density interactions. The noise in the self-energy stems from the stochastic nature of the CTQMC solver, and for frequencies above 20 eV there is no noise since we utilize the analytic form of Σ in the high-frequency limit. We note that the self-energy is well converged, particularly for low frequency.

For both CoO_2 and LiCoO_2 , $\text{Im}(\Sigma)$ goes to 0 at low frequency, consistent with well-defined quasiparticles and a band insulator, respectively. This indicates that CoO_2 can be described as a Fermi liquid and is not a Mott insulator, consistent with experiments on CoO_2 [62–64], whereas past DFT+ U studies predict an insulating state [19], as do our DFT+ U results in the present study. Therefore, DFT+DMFT is providing an improved description of the electronic structure of LCO. As a function of U , the magnitude of $\text{Im}(\Sigma)$ increases. The imaginary part of the self-energy is essentially identical for the E'_g and A_{1g} states, which indicates the symmetry breaking within the T_{2g} manifold is small. The overall magnitude of $\text{Im}(\Sigma)$ is moderately larger for CoO_2 than for LiCoO_2 . For CoO_2 , the imaginary part of the self-energy of the E'_g and A_{1g} states are larger in magnitude than those of the E_g states below $i\omega \approx 10$ eV, which is reasonable given their respective occupancies. The opposite trend is found for LiCoO_2 with a larger magnitude of $\text{Im}(\Sigma)$ for the E_g states for the full range of frequency shown. This suggests that for LiCoO_2 the correlations have a larger impact on the nominally unoccupied E_g states since they are partially occupied via

hybridization with O p states, whereas the E'_g and A_{1g} are filled.

For LiCoO_2 , in the high-frequency limit, $\text{Re}(\Sigma)$ is typically negative for E'_g and A_{1g} and positive for E_g . This indicates that the static part of the correlations tends to push E'_g and A_{1g} down in energy and E_g up in energy as is observed using $\text{DFT}+U$. The $U = 1.9$ eV case is an exception as J is likely too large relative to U in this case. The real part of the self-energy increases at lower frequency for E'_g and A_{1g} , whereas it decreases for E_g . This leads to a higher $\text{Re}(\Sigma)$ for E'_g and A_{1g} than E_g toward zero frequency. Overall, the magnitude of the changes in $\text{Re}(\Sigma)$ with U are significantly larger for E'_g and A_{1g} than for E_g .

For CoO_2 , the self-energy of the E_g states has a small real part (at most 0.21 eV), which decreases and becomes negative at low frequency. The magnitude is substantially larger for E'_g and A_{1g} than E_g with a maximum magnitude of 1.2 eV for $U = 5.9$ eV. For these states, like in the LiCoO_2 case, the values are negative at high frequency (except for very low U) and become positive at low frequency. As opposed to the imaginary part, the real part of the self-energy has smaller magnitude for CoO_2 than for LiCoO_2 .

From the low-frequency behavior of $\text{Im}(\Sigma)$, we compute the quasiparticle weight $Z = [1 - \partial \text{Im}(\Sigma)/\partial i\omega|_{i\omega \rightarrow 0}]^{-1}$, shown in Fig. 3. This quantity is unity for $U = J = 0$ [$\text{Im}(\Sigma) = 0$] and is inversely proportional to the effective mass arising from electron interactions. All the values decrease with U , as expected, in a roughly linear fashion. Z is always larger for LiCoO_2 than CoO_2 , consistent with the fact that LiCoO_2 is a band insulator. This effect is pronounced in the E'_g and A_{1g} states, for which the CoO_2 values are 0.14–0.20 lower than those of LiCoO_2 . For the E_g states, the disparity is smaller, with differences of only 0.01–0.04. For CoO_2 , Z is larger and decreases less rapidly for the E_g orbitals compared to the E'_g and A_{1g} orbitals. From $U = 1.9$ to 5.9 eV, Z of the E'_g and A_{1g} orbitals of CoO_2 goes from 0.79 to 0.57 and that of the E_g orbitals goes from 0.88 to 0.73. For LiCoO_2 , over the same range of U , Z of the E'_g and A_{1g} orbitals goes from 0.93 to 0.77 and that of the E_g orbitals goes from 0.89 to 0.77. Here, Z is smaller and decreases less rapidly for the E_g states such that Z is the same for all the orbitals at $U = 5.9$ eV.

B. Atomic configurations and d occupancies

To further understand the detailed electronic configuration of CoO_2 and LiCoO_2 , in Fig. 4 we plot the probabilities of the different atomic configurations sampled by the CTQMC solver in terms of the number of d electrons (N_d) and the spin projection S_z . The results for $U = 4.9$ eV are shown as a representative example. We note that the probability distribution is symmetric about $S_z = 0$ since our $\text{DFT}+\text{DMFT}$ calculations are paramagnetic (i.e., there is no long-range magnetic order).

Although CoO_2 and LiCoO_2 are nominally d^5 and d^6 , respectively, the probability distribution is centered at higher values of N_d for both cases due to the appreciable hybridization with O p states. For example, for LiCoO_2 there is substantial time in the Monte Carlo simulation in which an electron from an O p state has hopped into an E_g orbital, leading to a d^7 state. There are substantial fluctuations in N as well as S_z for

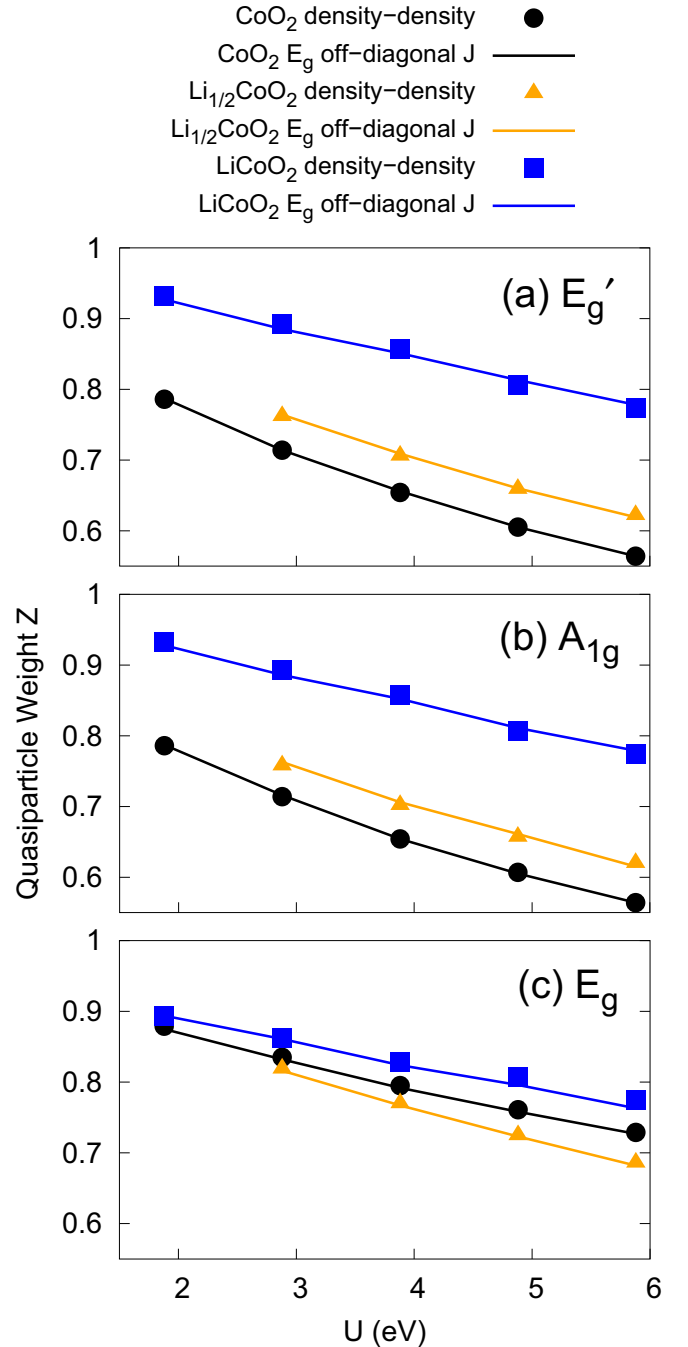


FIG. 3. Quasiparticle weight Z as a function of U for (a) E'_g , (b) A_{1g} , and (c) E_g orbitals in CoO_2 , $\text{Li}_{1/2}\text{CoO}_2$, and LiCoO_2 .

the Co site in both systems. For CoO_2 the spin fluctuations are moderately larger than in LiCoO_2 ; there is even probability of $S_z = \frac{3}{2}$ states. We note that these fluctuations of the Co site highlight why both DFT and $\text{DFT}+U$ struggle to capture all the physics in this system.

It is also useful to examine the behavior of N_d versus U for all the methodologies employed in this work in Fig. 5. This has been shown to give insight into the behavior and impact of the double-counting correction, which is purely a function of N_d [36,65,66]. Within DFT , one can observe that N_d is larger for the projector correlated subspace than the Wannier

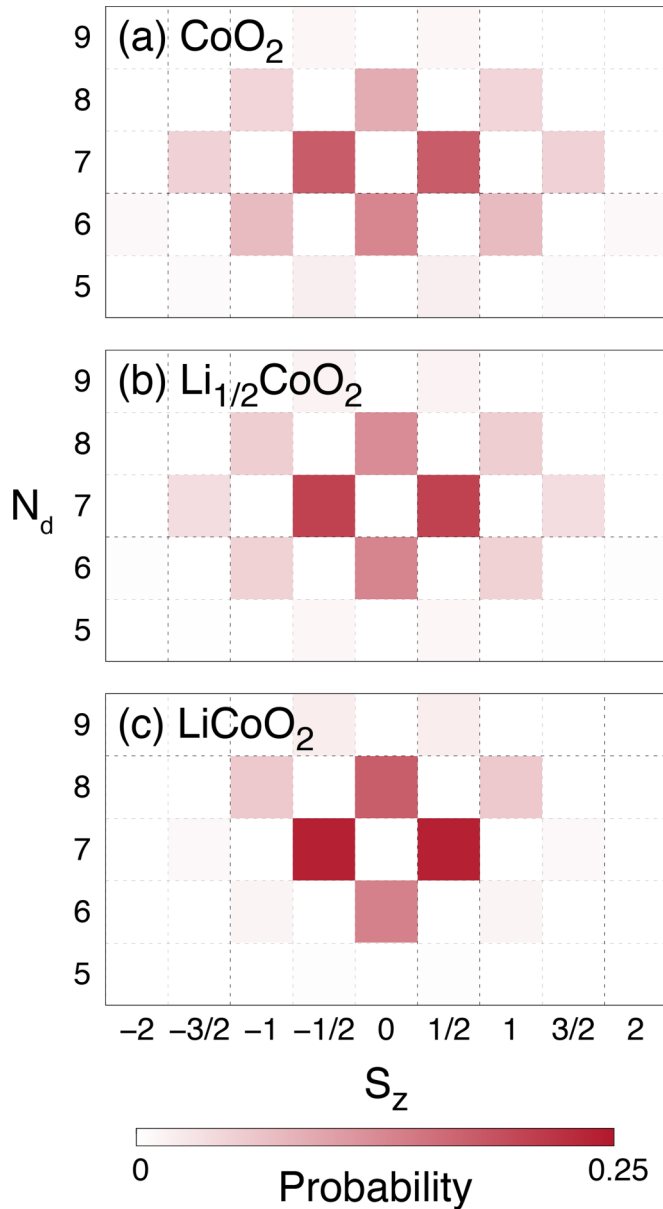


FIG. 4. Probability of Co atomic states with number of d electrons N_d and spin projection S_z for (a) CoO₂, (b) Li_{1/2}CoO₂, and (c) LiCoO₂.

correlated subspace. The difference is moderate for LiCoO₂ (0.09), but significantly larger for CoO₂ (0.26). LiCoO₂ has 0.08 (0.26) more d electrons than CoO₂ in the projector (Wannier) correlated subspace. These values are much smaller than the nominal value of unity, which is indicative of the strong p - d rehybridization in this system [7,67].

N_d typically decreases with U . When treating LiCoO₂ with DFT+ U in the Wannier correlated subspace, we find a transition to high-spin Co at U of around 4 eV. Since Co in LiCoO₂ is not high spin in experiments [15–17], we only consider the low-spin Co state to facilitate comparison with DFT+DMFT, for which we do not find this spurious high-spin state. For LiCoO₂ in the Wannier correlated subspace (the band insulator state), the decrease in N_d with U for DFT+ U is around 0.25 electrons. The inclusion of dynamical correlations (DFT+DMFT) substantially dampens this decrease to only 0.06 electrons. Unlike in the Wannier case, for DFT+ U in the projector correlated subspace, the decrease in N_d is small in magnitude (around 0.03 electrons) and including charge self-consistency leads to even smaller changes on the order of 0.006 electrons.

The behavior is similar for CoO₂. Here, DFT+DMFT gives a small decrease in N_d of 0.04 electrons, whereas the decrease is much more substantial (0.3 electrons) for DFT+ U in the Wannier correlated subspace, which describes CoO₂ as an insulator except for the smallest U considered. For DFT+ U in the projector case, in which there is a discontinuous decrease in N_d corresponding to a metal-insulator transition, charge self-consistency dampens the change in N_d from around 0.1 to 0.02 electrons.

The behavior of N_d versus U can further be understood by decomposing N_d into the components from the T_{2g} (E'_g and A_{1g}) and E_g orbitals, as shown in Fig. 6. We do not show the individual E'_g and A_{1g} occupancies for brevity, but they are included in the Supplemental Material [68]. Within DFT, the Wannier correlated subspace leads to higher (lower) occupancy of T_{2g} (E_g) by 0.13–0.23 (0.32–0.39) electrons compared to the projector case. In DFT+ U , the LiCoO₂ T_{2g} occupancy increases with U , whereas the E_g occupancy decreases more rapidly; this leads to the overall decrease in N_d . For the Wannier case, the T_{2g} occupancy increases more rapidly with U at lower U compared to the projector case; for larger U , the occupancy begins to saturate close to the nominal

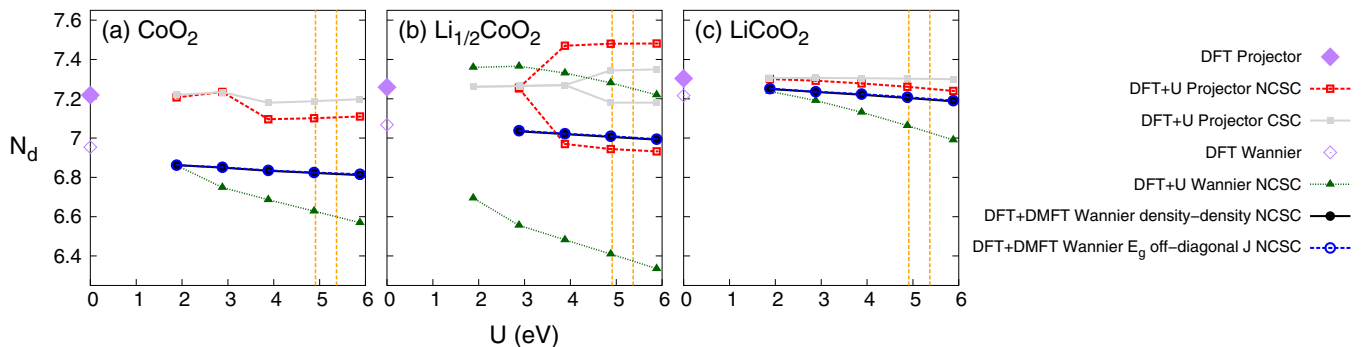


FIG. 5. N_d versus U for (a) CoO₂, (b) Li_{1/2}CoO₂, and (c) LiCoO₂ for all the methodologies employed in this study. The dashed orange lines indicate the computed values of U for LiCoO₂ (lower value) and CoO₂ (higher value) within the linear response approach. Multiple lines in (b) correspond to different values for the two Co sites.

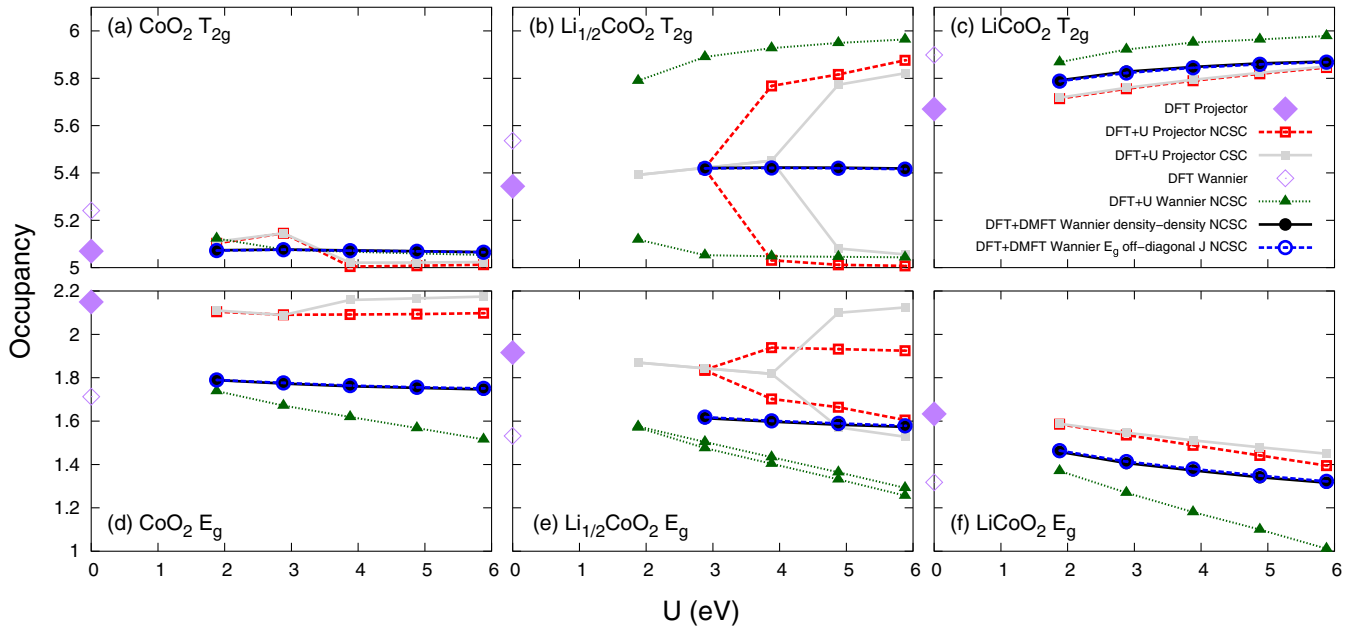


FIG. 6. Total T_{2g} occupancy versus U for (a) CoO_2 , (b) $\text{Li}_{1/2}\text{CoO}_2$, and (c) LiCoO_2 for all the methodologies employed in this study. (d)–(f) Show the corresponding E_g plots. Multiple lines in (b) and (e) correspond to different values for the two Co sites.

value of 6. Similarly, the decrease in E_g occupancy is more substantial in the Wannier case compared to the projector case. Including charge self-consistency has a very small effect on the occupancies of LiCoO_2 in the projector case. The trends in the occupancies are the same for DFT+DMFT as in DFT+ U , but the magnitude of the changes in occupancy is much smaller.

Within DFT+ U , the CoO_2 T_{2g} occupancy is relatively constant with U in the Wannier correlated subspace, whereas the E_g occupancy decreases by 0.22 electrons. The CoO_2 T_{2g} occupancy also does not change very much with U in the projector case, though there is a discontinuity leading to a decrease in occupancy through the metal-insulator transition. In this case, charge self-consistency serves to slightly enhance the T_{2g} and E_g occupancies. As in the case of LiCoO_2 , the changes in occupancy within DFT+DMFT are smaller than those of DFT+ U with both T_{2g} and E_g occupancies slightly decreasing by 0.003 and 0.04, respectively, over the range of U . We note that the DFT+DMFT occupancies are fairly similar to those of DFT for both CoO_2 and LiCoO_2 .

C. Electronic structure of $\text{Li}_{1/2}\text{CoO}_2$

Here, we discuss the electronic structure of $\text{Li}_{1/2}\text{CoO}_2$, which warrants extra attention due to the issue of spurious charge ordering which occurs in DFT+ U but is not seen experimentally [69]. This known structure has an in-plane ordering of Li corresponding to a primitive unit cell with two formula units [7,8,70]. We perform DFT+DMFT calculations in two different ways. First, we enforce the symmetry between the two structurally equivalent Co sites, i.e., only a single impurity problem is solved. However, the aforementioned approach does not allow for charge ordering to spontaneously break point symmetry. Therefore, we also use a second approach where two impurity calculations are employed (i.e.,

one for each Co atom in the unit cell), and we only execute this at $U = 3.9$ eV due to computational expense. Using the second approach, we do find a stable charge-ordered state, with a difference in N_d on the two sites of 0.4 electrons, but it is slightly higher in energy than the non-charge-ordered state (by 3 meV/f.u.). Although this is a quite small energy difference, it is clear that DFT+DMFT removes the strong tendency for spurious charge ordering that is produced by DFT+ U , and we proceed with our analysis of the symmetric solution.

Within DFT, $\text{Li}_{1/2}\text{CoO}_2$ is metallic with half a hole in the T_{2g} manifold, as can be seen from the density of states in Fig. 1(b). For DFT+ U in the Wannier correlated subspace, like in the LiCoO_2 case (discussed above), we ignore states containing high-spin Co found at large U ; instead, we consider the low-spin ground state, a charge-ordered insulator [see Figs. 5(b), 6(b), and 6(e)]. Within DFT+ U in the projector correlated subspace, $\text{Li}_{1/2}\text{CoO}_2$ is in a symmetric low-spin state at low U that transitions to a low-spin charge-ordered insulator at larger U . The DFT+DMFT self-energy in Fig. 2 illustrates that $\text{Li}_{1/2}\text{CoO}_2$ is, like CoO_2 , a Fermi liquid with correlations most significantly affecting the T_{2g} manifold. We find a Fermi liquid up to the highest U value considered, in agreement with the metallic behavior observed in experiment [52,71,72]. The T_{2g} quasiparticle weights, in Fig. 3, are significantly lower than those of LiCoO_2 and slightly larger than those of CoO_2 . This reflects that the electronic structure of $\text{Li}_{1/2}\text{CoO}_2$ is closer to that of CoO_2 than LiCoO_2 .

As for the end members ($x = 0$ and 1), for $\text{Li}_{1/2}\text{CoO}_2$, N_d (Fig. 5) is larger in the projector correlated subspace. Within DFT+DMFT, N_d decreases very mildly with U similar to the end-member behavior. Here, dynamical correlations only slightly reduce N_d (on the order of 0.02 electrons). Within NCSC DFT+ U , the magnitude of the charge ordering is substantial (as much as ~ 0.8 electrons) in the Wannier correlated

subspace. It is significantly smaller for the projector case, and is further dampened by charge self-consistency. Similar effects are found for the individual T_{2g} and E_g occupancies are shown in Fig. 6.

In summary, DFT+DMFT can properly describe the electronic structure of $\text{Li}_{1/2}\text{CoO}_2$. Unlike DFT+ U , which predicts a charge-ordered insulator, DFT+DMFT properly describes the electronic structure as a Fermi liquid without a strong tendency for charge ordering.

D. Total energy of LiCoO_2 and CoO_2

Having documented the basic electronic structure, we proceed to explore the total energy of LiCoO_2 and CoO_2 as a function of U , allowing for a direct comparison between DFT+DMFT and DFT+ U . The total energy of LCO is shown as a function of U for several methodologies in Fig. 7. The two vertical dashed lines indicate the values of U for CoO_2 and LiCoO_2 as computed from first principles via linear response [73]. The total energies increase with U , as expected. We note that extrapolating any of the results to $U = 0$ does not approach the DFT result (large purple diamond), which is simply due to the fact that we used a fixed value of J for all calculations. The magnitude of the increase in total energy with U is generally greater for CoO_2 than LiCoO_2 , which makes sense since the impact of the onsite interaction is expected to be larger for the system for which T_{2g} is partially filled (nominally). For NCSC DFT+ U in the Wannier correlated subspace, for example, over the full range of U shown, the increase in energy of CoO_2 is 2.4 eV as compared to only 1.8 eV for LiCoO_2 . For the same set of calculations using the projector correlated subspace, we find the same trend with energy increases of roughly 2.7 eV for CoO_2 and 2.3 eV for LiCoO_2 . We note that the individual total energies from methods utilizing these different correlated subspaces (projector and Wannier) are not directly comparable, but the behavior of the total energy with U is similar.

We estimate the magnitude of the error associated with neglecting charge self-consistency via DFT+ U calculations in the projector correlated subspace. Here, for LiCoO_2 , we find only very small differences (at most 9 meV/f.u.) between the NCSC and CSC total energies. For CoO_2 , the situation is similar with differences in total energy of at most 20 meV/f.u. The small impact of changes in charge density on the total energies suggest the fixed charge density should be a reasonable approximation for DFT+DMFT. More importantly, we have a clear guideline on the magnitude of the effect for charge self-consistency within DFT+ U , and we expect this is an upper bound for DFT+DMFT calculations in which the impact will likely be dampened.

Within DFT+DMFT, we find very little impact of including the off-diagonal J interaction terms within the E_g manifold in addition to the density-density interactions. The magnitude of the differences is typically only around 5–15 meV/f.u. for LiCoO_2 and 3–9 meV/f.u. for CoO_2 . This suggests that density-density interactions are likely sufficient to describe this class of systems. In all of the following results, we find no significant difference in employing these two interaction forms. The DFT+DMFT results, which employ the Wannier correlated subspace, appear to merge with the corresponding

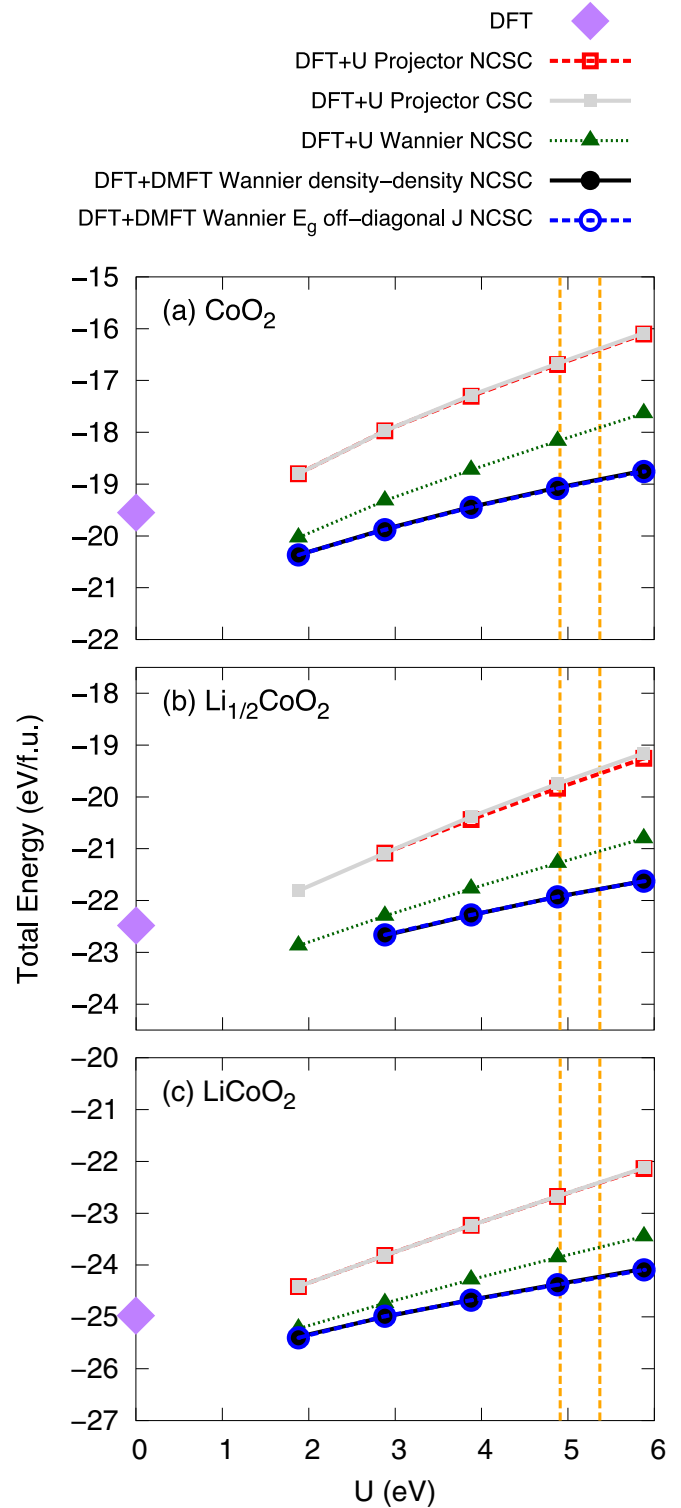


FIG. 7. Total energy of (a) CoO_2 , (b) $\text{Li}_{1/2}\text{CoO}_2$, and (c) LiCoO_2 , respectively, as a function of U for several methodologies including DFT, DFT+ U , and DFT+DMFT (J remains unchanged). The dashed orange lines indicate the computed values of U for LiCoO_2 (lower value) and CoO_2 (higher value) within the linear response approach.

DFT+ U results in the limit of small U , as should be the case. We note again that in this limit, neither the DFT+ U nor the DFT+DMFT results recover the DFT values (large purple

diamonds in Fig. 7) simply because we have taken a fixed finite J value, whereas the DFT values correspond to $J = 0$.

We find the general impact of dynamical correlations on the energetics is to dampen the magnitude of the increase in total energy with U as compared to the static Hartree-Fock treatment in DFT+ U . When U is increased from 1.9 to 5.9 eV, the total energy of LiCoO₂ increases by 1.8 eV within DFT+ U as opposed to only 1.3 eV within DFT+DMFT. For CoO₂, the magnitude of these energies is substantially larger with an increase of 2.4 eV for DFT+ U and 1.6 eV for DFT+DMFT. By this measure, dynamical correlations decrease the energy penalty of U by 26% for LiCoO₂ and 33% for CoO₂. Therefore, dynamical correlations have a larger impact on CoO₂ than LiCoO₂. This corresponds to very large absolute differences in the energies predicted by DFT+ U and DFT+DMFT. For CoO₂, for example, around the linear response values of U the difference in energy is around 1 eV. This strongly suggests dynamical correlations, missing in the DFT+ U approach, are important for accurate total energies.

It should be emphasized that the difference between DFT+DMFT and DFT+ U changes substantially as a function of x , and this error will therefore strongly affect observables. One strategy to correct errors within DFT+ U calculations is to tune U to artificially low values, and this can be successful if U is first calibrated to some experimental observable. However, our work indicates that the errors vary strongly with composition and, therefore, DFT+ U studies of compositional phase stability would need to tune U as a function of doping, a far more challenging task. Below, we explore the average battery voltage, where the composition-dependent errors within DFT+ U have severe consequences.

E. Average intercalation voltage

We turn our attention to the average intercalation voltage of LCO for $0 \leq x \leq 1$, plotted in Fig. 8, which is a key observable for a rechargeable battery cathode. The average intercalation voltage V is computed via $eV = E(\text{Li}) + E(\text{CoO}_2) - E(\text{LiCoO}_2)$, where e is the elementary charge and body-centered-cubic Li is the reference electrode [6]. As has been known, DFT tends to underpredict the experimental voltage [6], in this case by around 0.7 V. The predicted voltage increases with DFT+ U . In the projector correlated subspace, the value comes close to reasonable agreement with the experimental value (approximately 4.26 V [74]) for the largest U considered, and charge self-consistency has a negligible effect. The voltage also becomes larger than the DFT value for DFT+ U in the Wannier case, though the predicted values are appreciably smaller and do not reach agreement with experiment. In stark contrast, within DFT+DMFT, the predicted intercalation voltage is smaller than the DFT value up to the highest computed value of $U = 6$ eV. As compared to DFT+ U , the voltage at fixed J increases much more slowly as a function of U . This mainly stems from the dampened increase in energy for CoO₂. For the computed values of U , the predicted voltage is only 3.39–3.45 V, a moderate amount less than that of pure DFT.

The increase in V within DFT+ U and general agreement with experiment was shown previously [73] and seemed to suggest that DFT+ U is reliable for this class of materials.

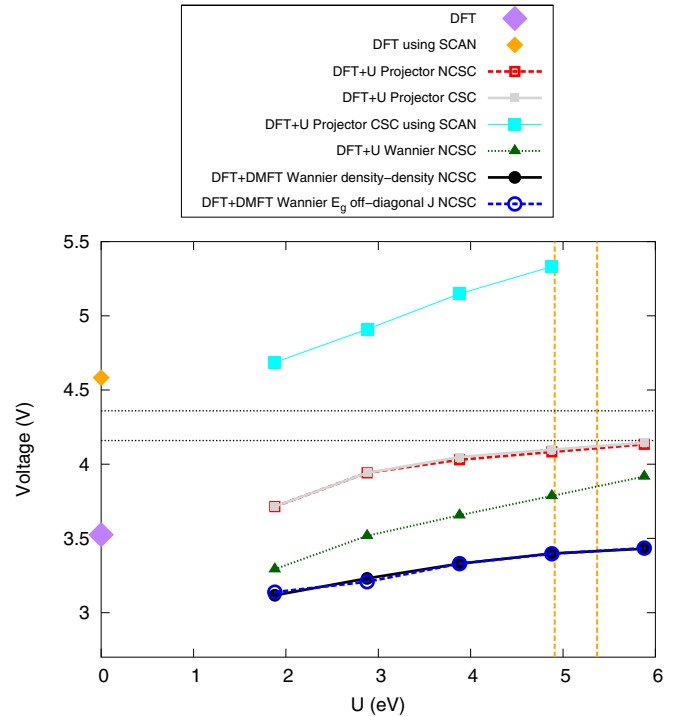


FIG. 8. Computed intercalation voltage of LCO via DFT, DFT+ U , and DFT+DMFT as a function of U . The dashed orange lines indicate the computed values of U for LiCoO₂ (lower value) and CoO₂ (higher value) within the linear response approach. The dotted black lines indicate the expected range of the experimental result [74].

However, this viewpoint should be carefully scrutinized given that DFT+ U is a rather crude theory, in that DFT+ U is obtained from DFT+DMFT when the quantum impurity problem is solved within static mean-field theory, neglecting dynamical correlations. Therefore, DFT+DMFT is superior in every respect. Since the voltage curve predicted by DFT+DMFT produces a result smaller than that of DFT, opposite to that of DFT+ U , dynamical correlations are clearly essential to describe the energetics of LCO. The fact that DFT+ U increases the voltage, relative to DFT, and provides more reasonable agreement with experiment appears to be fortuitous.

Given that DFT+DMFT actually worsens the predicted voltage as compared to DFT, we are left with the puzzling question as to why. We explore several possibilities. First and foremost, while DMFT should improve DFT with respect to local physics, it is possible that there are still substantial nonlocal errors within the density functional employed in the DFT+DMFT functional. Given the recent successes of the relatively new SCAN functional [75,76], which contains nonlocal physics via a dependence on the orbital kinetic energy density, an obvious question is how the voltage would change if we replaced the PBE functional with SCAN; we pursue this idea at the level of DFT+ U (see Fig. 8). The $U = 0$ voltage predicted by SCAN is 4.58 V, which is already greater than the experimental voltage, in stark contrast to LDA and PBE. One expects the trends as a function of U for DFT(SCAN)+ U and DFT(SCAN)+DMFT to be unchanged

relative to PBE given that the SCAN electronic structure is very similar to that of PBE. As expected, increasing U within DFT(SCAN)+ U causes the voltage to further increase, moving away from the experimental value. We do not compute the DFT(SCAN)+DMFT results due to the computational cost, but we anticipate that they should have the same U dependence as DFT(PBE)+DMFT, just as DFT(SCAN)+ U and DFT(PBE)+ U have a very similar U dependence. If so, the DFT(SCAN)+DMFT voltage should be mildly decreased compared to the DFT(SCAN) voltage, yielding reasonable agreement with experiment. Alternatively, DFT(SCAN)+ U only worsens the voltage prediction, and this suggests the reason why DFT(PBE)+ U performs well is due to the cancellations of two large and distinct errors. Therefore, our results suggest one cannot expect DFT+ U to perform as a predictive tool in the context of compositional phase stability.

Of course, another factor to consider is that the precise value of the predicted voltage will depend on the precise values U and J . Allowing for small U differences in the end members will result in small changes in the voltage. Similar arguments might be made for other uncertainties in the methodology, such as the double-counting correction, etc. We do not attempt to build a case for the most correct set of parameters in this work. It is worth noting that one early explanation for discrepancies in the DFT predicted voltages was the overestimated magnitude of the cohesive energy of body-centered-cubic Li within LDA [6]. However, we find the cohesive energy predicted by PBE (-1.60 eV) and SCAN (-1.59 eV) are in good agreement with experiment (-1.63 eV [77]). Therefore, the discrepancy between theory and experiment should stem from the energetics of the cathode material itself.

F. Phase stability of $\text{Li}_{1/2}\text{CoO}_2$

As another test of the computed DFT+DMFT total energy, we compute the phase stability of $\text{Li}_{1/2}\text{CoO}_2$. The formation energy ΔE , computed as $E(\text{Li}_{1/2}\text{CoO}_2) - \frac{1}{2}[E(\text{CoO}_2) + E(\text{LiCoO}_2)]$, is shown in Fig. 9. We use the difference in average experimental voltage values for $0 < x < \frac{1}{2}$ (V_-) and $\frac{1}{2} < x < 1$ (V_+) to estimate the experimental formation energy for $x = \frac{1}{2}$, via $\Delta E = x(1-x)(eV_+ - eV_-)$ [78]. Using the data of Ref. [74], we compute ΔE of -114 meV/f.u. for $\text{Li}_{1/2}\text{CoO}_2$. As the formation energy has a significantly smaller scale than the voltage, it is more sensitive to the different methodologies employed in this work. Furthermore, the energetics of NCSC calculations will be less reliable when there is a substantial rearrangement of charge.

We find a DFT value of -218 meV/f.u. NCSC DFT+ U in the projector correlated subspace significantly decreases the magnitude of the formation energy and nearly reaches agreement with experiment at large U . Charge self-consistency tends to destabilize $\text{Li}_{1/2}\text{CoO}_2$ compared to the end members, further lowering the formation energy magnitude to values much smaller than experiment. While the formation energy remains negative (in agreement with the experimentally known phase stability), we have shown previously that the more common DFT+ U methodology based on spin-dependent DFT incorrectly predicts phase separation of $\text{Li}_{1/2}\text{CoO}_2$ in the absence of charge ordering [13]. The formation energy is also

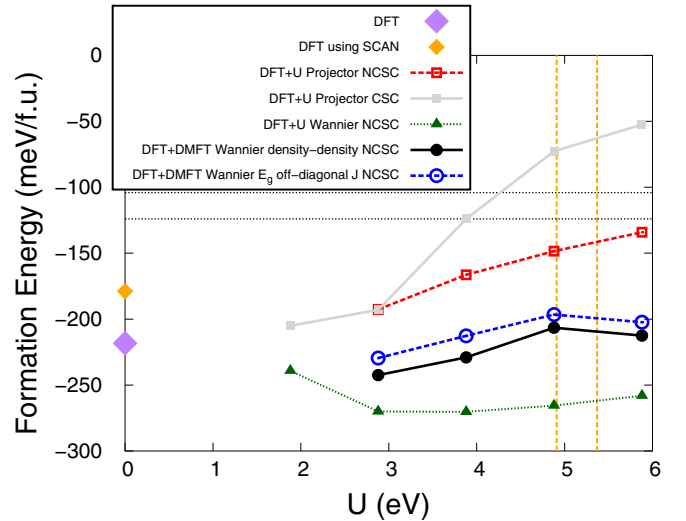


FIG. 9. Computed formation energy of $\text{Li}_{1/2}\text{CoO}_2$ via DFT, DFT+ U , and DFT+DMFT as a function of U . The dashed orange lines indicate the computed values of U for LiCoO_2 (lower value) and CoO_2 (higher value) within the linear response approach. The dotted black lines indicate the expected range of the experimental result [74].

significantly affected by U using DFT+ U in the Wannier correlated subspace, but in the opposite direction. In this case, the formation energy is pushed more negative to values of 260 – 270 meV/f.u.

Given that DFT+DMFT prefers not to charge order, the errors associated with NCSC are expected to be comparable to those estimated for the end members, which would still be small on this scale. DFT+DMFT shows only a small increase in formation energy with U , on the order of tens of meV/f.u. The predicted value in the range of computed U is similar to that of DFT. The DFT+DMFT error may also be associated in part with the DFT exchange–correlation functional. We also plot the formation energy using the SCAN functional, which is approximately 50 meV/f.u. higher than the PBE value. Therefore, we would anticipate the DFT(SCAN)+DMFT results to be shifted by roughly the same amount, which would be much closer to the experimental range. In summary, similar to the voltage behavior, our results suggest that dynamical correlations significantly impact the predicted formation energy and that DFT+DMFT based on SCAN will lead to improved agreement with experiment.

IV. CONCLUSIONS

We investigate the electronic structure, intercalation voltage, and phase stability of LCO with the many-body DFT+DMFT methodology and compare to DFT and DFT+ U . In DFT+DMFT, LiCoO_2 is a band insulator, while we find that CoO_2 and $\text{Li}_{1/2}\text{CoO}_2$ are moderately correlated Fermi liquids, without a strong tendency for charge ordering in $\text{Li}_{1/2}\text{CoO}_2$, in agreement with experiments. Dynamical correlations (missing in DFT+ U) substantially impact the energetics of LCO by dampening the changes in total energy and N_d found via the DFT+ U approach, especially for CoO_2 and $\text{Li}_{1/2}\text{CoO}_2$. The intercalation voltage behavior of DFT+ U

and DFT+DMFT is qualitatively different, with the latter decreasing the voltage with respect to DFT; the phase stability of $\text{Li}_{1/2}\text{CoO}_2$ within DFT+DMFT also differs starkly from DFT+ U . DFT+DMFT calculations based on the PBE GGA DFT functional underpredict the voltage and overestimate the stability of $\text{Li}_{1/2}\text{CoO}_2$ compared to experiment; we find evidence that DFT+DMFT based on the more accurate SCAN DFT functional will lead to significantly closer agreement to experiment.

We find that dynamical correlations are important to describe this class of materials despite the relatively modest quasiparticle weights. Our results suggest that the Hartree-Fock treatment of the impurity problem in DFT+ U is insufficient to accurately describe the electronic structure and thermodynamics of correlated electron materials. In addition, due to the strong composition dependence of the impact of dynamical correlations, our results challenge the common practice of artificially tuning U within DFT+ U to compensate for the errors of Hartree-Fock. Given the significant computational

expense of solving the impurity problem in DFT+DMFT, the development of less computationally expensive but still sufficiently accurate impurity solvers will be important future work to enable the study of compositional phase stability of strongly correlated electron materials.

ACKNOWLEDGMENTS

We acknowledge H. Park (UIC/Argonne) for useful discussions. This research used resources of the National Energy Research Scientific Computing Center, a DOE Office of Science User Facility supported by the Office of Science of the U.S. Department of Energy under Contract No. DE-AC02-05CH11231. E.B.I. gratefully acknowledges the U.S. Department of Energy Computational Science Graduate Fellowship (Grant No. DE-FG02-97ER25308) for support. C.A.M. was supported by the Grant No. DE-SC0016507 funded by the U.S. Department of Energy, Office of Science.

-
- [1] G. Kotliar and D. Vollhardt, *Phys. Today* **57**(3), 53 (2004).
- [2] E. Morosan, D. Natelson, A. H. Nevidomskyy, and Q. Si, *Adv. Mater.* **24**, 4896 (2012).
- [3] M. S. Whittingham, *Chem. Rev.* **104**, 4271 (2004).
- [4] K. Mizushima, P. Jones, P. Wiseman, and J. Goodenough, *Mater. Res. Bull.* **15**, 783 (1980).
- [5] M. T. Czyżyk, R. Potze, and G. A. Sawatzky, *Phys. Rev. B* **46**, 3729 (1992).
- [6] M. K. Aydinol, A. F. Kohan, G. Ceder, K. Cho, and J. Joannopoulos, *Phys. Rev. B* **56**, 1354 (1997).
- [7] C. Wolverton and A. Zunger, *Phys. Rev. Lett.* **81**, 606 (1998).
- [8] A. Van der Ven, M. K. Aydinol, G. Ceder, G. Kresse, and J. Hafner, *Phys. Rev. B* **58**, 2975 (1998).
- [9] P. Hohenberg and W. Kohn, *Phys. Rev.* **136**, B864 (1964).
- [10] W. Kohn and L. J. Sham, *Phys. Rev.* **140**, A1133 (1965).
- [11] V. L. Chevrier, S. P. Ong, R. Armiento, M. K. Y. Chan, and G. Ceder, *Phys. Rev. B* **82**, 075122 (2010).
- [12] A. I. Liechtenstein, V. I. Anisimov, and J. Zaanen, *Phys. Rev. B* **52**, R5467 (1995).
- [13] E. B. Isaacs and C. A. Marianetti, *Phys. Rev. B* **95**, 045141 (2017).
- [14] B. Andriyevsky, K. Doll, and T. Jacob, *Phys. Chem. Chem. Phys.* **16**, 23412 (2014).
- [15] J. van Elp, J. L. Wieland, H. Eskes, P. Kuiper, G. A. Sawatzky, F. M. F. de Groot, and T. S. Turner, *Phys. Rev. B* **44**, 6090 (1991).
- [16] M. Ménétrier, I. Saadoune, S. Levasseur, and C. Delmas, *J. Mater. Chem.* **9**, 1135 (1999).
- [17] M. Ménétrier, D. Carlier, M. Blangero, and C. Delmas, *Electrochem. Solid-State Lett.* **11**, A179 (2008).
- [18] D.-H. Seo, A. Urban, and G. Ceder, *Phys. Rev. B* **92**, 115118 (2015).
- [19] P. Zhang, W. Luo, V. H. Crespi, M. L. Cohen, and S. G. Louie, *Phys. Rev. B* **70**, 085108 (2004).
- [20] G. Kotliar, S. Y. Savrasov, K. Haule, V. S. Oudovenko, O. Parcollet, and C. A. Marianetti, *Rev. Mod. Phys.* **78**, 865 (2006).
- [21] S. Y. Savrasov, G. Kotliar, and E. Abrahams, *Nature (London)* **410**, 793 (2001).
- [22] K. Held, A. K. McMahan, and R. T. Scalettar, *Phys. Rev. Lett.* **87**, 276404 (2001).
- [23] X. Dai, S. Y. Savrasov, G. Kotliar, A. Migliori, H. Ledbetter, and E. Abrahams, *Science* **300**, 953 (2003).
- [24] A. K. McMahan, *Phys. Rev. B* **72**, 115125 (2005).
- [25] B. Amadon, S. Biermann, A. Georges, and F. Aryasetiawan, *Phys. Rev. Lett.* **96**, 066402 (2006).
- [26] L. V. Pourovskii, B. Amadon, S. Biermann, and A. Georges, *Phys. Rev. B* **76**, 235101 (2007).
- [27] I. Leonov, N. Binggeli, D. Korotin, V. I. Anisimov, N. Stojić, and D. Vollhardt, *Phys. Rev. Lett.* **101**, 096405 (2008).
- [28] I. Di Marco, J. Minár, S. Chadov, M. I. Katsnelson, H. Ebert, and A. I. Liechtenstein, *Phys. Rev. B* **79**, 115111 (2009).
- [29] I. Leonov, D. Korotin, N. Binggeli, V. I. Anisimov, and D. Vollhardt, *Phys. Rev. B* **81**, 075109 (2010).
- [30] J. Kuneš, I. Leonov, M. Kollar, K. Byczuk, V. I. Anisimov, and D. Vollhardt, *Eur. Phys. J. Spec. Top.* **180**, 5 (2009).
- [31] M. Aichhorn, L. Pourovskii, and A. Georges, *Phys. Rev. B* **84**, 054529 (2011).
- [32] I. Leonov, A. I. Poteryaev, V. I. Anisimov, and D. Vollhardt, *Phys. Rev. B* **85**, 020401(R) (2012).
- [33] D. Grieger, C. Piefke, O. E. Peil, and F. Lechermann, *Phys. Rev. B* **86**, 155121 (2012).
- [34] J. Bieder and B. Amadon, *Phys. Rev. B* **89**, 195132 (2014).
- [35] N. Zaki, H. Park, R. M. Osgood, A. J. Millis, and C. A. Marianetti, *Phys. Rev. B* **89**, 205427 (2014).
- [36] H. Park, A. J. Millis, and C. A. Marianetti, *Phys. Rev. B* **90**, 235103 (2014).
- [37] H. Park, A. J. Millis, and C. A. Marianetti, *Phys. Rev. B* **89**, 245133 (2014).
- [38] J. Chen, A. J. Millis, and C. A. Marianetti, *Phys. Rev. B* **91**, 241111(R) (2015).
- [39] K. Haule and T. Birol, *Phys. Rev. Lett.* **115**, 256402 (2015).
- [40] P. Delange, T. Ayrál, S. I. Simak, M. Ferrero, O. Parcollet, S. Biermann, and L. Pourovskii, *Phys. Rev. B* **94**, 100102(R) (2016).
- [41] K. Haule and G. L. Pascut, *Sci. Rep.* **7**, 10375 (2017).
- [42] K. Haule, *J. Phys. Soc. Jpn.* **87**, 041005 (2018).

- [43] Q. Han, T. Birol, and K. Haule, *Phys. Rev. Lett.* **120**, 187203 (2018).
- [44] J. P. Perdew, K. Burke, and M. Ernzerhof, *Phys. Rev. Lett.* **77**, 3865 (1996).
- [45] P. E. Blöchl, *Phys. Rev. B* **50**, 17953 (1994).
- [46] G. Kresse and D. Joubert, *Phys. Rev. B* **59**, 1758 (1999).
- [47] G. Kresse and J. Hafner, *Phys. Rev. B* **49**, 14251 (1994).
- [48] G. Kresse and J. Hafner, *Phys. Rev. B* **47**, 558 (1993).
- [49] G. Kresse and J. Furthmüller, *Phys. Rev. B* **54**, 11169 (1996).
- [50] G. Kresse and J. Furthmüller, *Comput. Mater. Sci.* **6**, 15 (1996).
- [51] J. Sun, A. Ruzsinszky, and J. P. Perdew, *Phys. Rev. Lett.* **115**, 036402 (2015).
- [52] T. Motohashi, T. Ono, Y. Sugimoto, Y. Masubuchi, S. Kikkawa, R. Kanno, M. Karppinen, and H. Yamauchi, *Phys. Rev. B* **80**, 165114 (2009).
- [53] A. A. Mostofi, J. R. Yates, Y.-S. Lee, I. Souza, D. Vanderbilt, and N. Marzari, *Comput. Phys. Commun.* **178**, 685 (2008).
- [54] K. Haule, *Phys. Rev. B* **75**, 155113 (2007).
- [55] E. Gull, A. J. Millis, A. I. Lichtenstein, A. N. Rubtsov, M. Troyer, and P. Werner, *Rev. Mod. Phys.* **83**, 349 (2011).
- [56] O. Bengone, M. Alouani, P. Blöchl, and J. Hugel, *Phys. Rev. B* **62**, 16392 (2000).
- [57] E. Pavarini, E. Koch, D. Vollhardt, and A. Lichtenstein, *The LDA+DMFT Approach to Strongly Correlated Materials: Lecture Notes of the Autumn School*, Schriften des Forschungszentrums Jülich. Reihe Modeling and simulation, Vol. 1 (Forschungszentrum, Zentralbibliothek, 2011).
- [58] K. Haule, C.-H. Yee, and K. Kim, *Phys. Rev. B* **81**, 195107 (2010).
- [59] M. Schüler, O. E. Peil, G. J. Krabberger, R. Pordzik, M. Marsman, G. Kresse, T. O. Wehling, and M. Aichhorn, *J. Phys.: Condens. Matter* **30**, 475901 (2018).
- [60] V. I. Anisimov, I. V. Solovyev, M. A. Korotin, M. T. Czyżyk, and G. A. Sawatzky, *Phys. Rev. B* **48**, 16929 (1993).
- [61] K. Momma and F. Izumi, *J. Appl. Crystallogr.* **44**, 1272 (2011).
- [62] C. de Vaulx, M.-H. Julien, C. Berthier, S. Hébert, V. Pralong, and A. Maignan, *Phys. Rev. Lett.* **98**, 246402 (2007).
- [63] T. Motohashi, Y. Katsumata, T. Ono, R. Kanno, M. Karppinen, and H. Yamauchi, *Chem. Mater.* **19**, 5063 (2007).
- [64] S. Kawasaki, T. Motohashi, K. Shimada, T. Ono, R. Kanno, M. Karppinen, H. Yamauchi, and G.-q. Zheng, *Phys. Rev. B* **79**, 220514(R) (2009).
- [65] X. Wang, M. J. Han, L. de' Medici, H. Park, C. A. Marianetti, and A. J. Millis, *Phys. Rev. B* **86**, 195136 (2012).
- [66] H. T. Dang, X. Ai, A. J. Millis, and C. A. Marianetti, *Phys. Rev. B* **90**, 125114 (2014).
- [67] C. A. Marianetti, G. Kotliar, and G. Ceder, *Phys. Rev. Lett.* **92**, 196405 (2004).
- [68] See Supplemental Material at <http://link.aps.org/supplemental/10.1103/PhysRevB.102.045146> for crystal structure details and a breakdown of N_d into the E'_g , A_{1g} , and E_g occupancies.
- [69] Y. Takahashi, N. Kijima, K. Tokiwa, T. Watanabe, and J. Akimoto, *J. Phys.: Condens. Matter* **19**, 436202 (2007).
- [70] J. N. Reimers and J. R. Dahn, *J. Electrochem. Soc.* **139**, 2091 (1992).
- [71] K. Miyoshi, C. Iwai, H. Kondo, M. Miura, S. Nishigori, and J. Takeuchi, *Phys. Rev. B* **82**, 075113 (2010).
- [72] T. Y. Ou-Yang, F.-T. Huang, G. J. Shu, W. L. Lee, M.-W. Chu, H. L. Liu, and F. C. Chou, *Phys. Rev. B* **85**, 035120 (2012).
- [73] F. Zhou, M. Cococcioni, C. A. Marianetti, D. Morgan, and G. Ceder, *Phys. Rev. B* **70**, 235121 (2004).
- [74] G. G. Amatucci, J. M. Tarascon, and L. C. Klein, *J. Electrochem. Soc.* **143**, 1114 (1996).
- [75] E. B. Isaacs and C. Wolverton, *Phys. Rev. Mater.* **2**, 063801 (2018).
- [76] Y. Zhang, D. A. Kitchaev, J. Yang, T. Chen, S. T. Dacek, R. A. Sarmiento-Pérez, M. A. L. Marques, H. Peng, G. Ceder, J. P. Perdew, and J. Sun, *npj Computat. Mater.* **4**, 9 (2018).
- [77] C. Kittel, *Introduction to Solid State Physics*, 6th ed. (Wiley, New York, 1986).
- [78] M. Aykol and C. Wolverton, *Phys. Rev. B* **90**, 115105 (2014).